THE JOURNAL OF PHYSICAL CHEMISTRY B

Article

pubs.acs.org/JPCB

Toward Vibrational Dynamics at Liquid−Liquid and Nano-Interfaces: Time-Resolved Sum-Frequency Scattering

Rüdiger Scheu and Sylvie Roke*

Laboratory of fundamental BioPhotonics (LBP), Institute of Bioengineering (IBI), School of Engineering, École Polytechnique Fédérale de Lausanne (EPFL), 1015 Lausanne, Switzerland

ABSTRACT: Interfacial molecular dynamics are key to understanding many phenomena in technology and life sciences. We demonstrate a first step toward accessing vibrational dynamics at liquid−liquid and nanoscopic (bio)-interfaces using time-resolved sum-frequency scattering to probe the interfaces of a nanodroplet platform. The free induction decay of the vibrational modes of dodecylsulfate amphiphiles from the interface of dispersed nanoscopic oil droplets was measured. We probed the vibrational response of both the functional headgroup and the alkyl tail of the amphiphiles. In the molecular fingerprint region, a beating of vibrational modes was observed. Simultaneous modeling of the time- and frequency-resolved response revealed modes at ∼995 and ∼1065 cm^{-1} that can be assigned to C−O−S and SO_3 stretch vibrations.

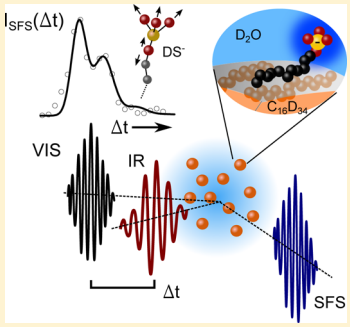

INTRODUCTION

Time-resolved femtosecond vibrational spectroscopy is a valuable tool to study condensed phases. It provides information on the structure and dynamics of molecules on time scales relevant for many biological and chemical processes.[1] Particularly important are the structure and dynamics at interfaces[2−7] because they play a key role in phenomena such as molecular transport, catalysis, or self-assembly. Moreover, the dynamics at interfaces often greatly differ from bulk dynamics; for example, water reorientation is much faster at the air−water interface than in bulk water.[8]

Interfacial relaxation dynamics can be revealed by time-domain vibrational sum-frequency generation (SFG).[9,10] In particular, SFG free induction decay (SFG-FID)[11,12] techniques that probe the dephasing of vibrational modes have been employed to study adsorbates at metal interfaces,[13−15] water at the D_2O−CaF_2 interface[16] as well as Langmuir−Blodgett and self-assembled monolayers.[17,18] Though SFG is thus extremely powerful in elucidating dynamics at a variety of interfaces, its application has been restricted to planar vapor−liquid, solid−liquid, and solid−solid interfaces,[2,9] which are easily accessible by optical beams. Vibrational dynamics at liquid−liquid interfaces are more challenging to probe in planar geometries and have thus not been characterized yet. Furthermore, many biologically and chemically important interfaces such as those of proteins, vesicles, and colloids are structured on the nanoscale. To access them, SFG can be combined with light scattering techniques, thereby extending its application to nanoscopic systems and aqueous dispersions. Sum-frequency scattering (SFS) has thus been used to study the structure of nanoscopic colloidal particles, liquid nanodroplets, and catanionic vesicles.[12,19,20] SFS in combination with the nanodroplet dispersion platform also has the advantage that it facilitates the measurement of liquid−liquid interfaces and that it is less prone to impurities because of the large surface-to-volume ratios in nanoscopic dispersions.[21,22] Extending SFS to the time domain would be key to access the dynamics of molecules at nanoscopic biointerfaces, liquid−liquid and nanoparticle interfaces.

Here, we demonstrate a time-resolved sum-frequency-scattering (TD-SFS) experiment. We recorded the free induction decay (FID) of the vibrational modes of dodecylsulfate (DS^-) amphiphiles adsorbed to the interface of dispersed nanoscopic oil droplets in aqueous solution. We probed the vibrational response of both the head groups and the alkyl tails of the amphiphiles. In the molecular fingerprint region around ∼1000 cm^{-1}, we observed a beating on the time-domain signal, indicating that two sum-frequency-active modes coherently interfere; the symmetric stretch mode of the SO_3^- headgroup and another mode that we tentatively assign to a C−O−S stretch vibration.

In the following we will first describe sample preparation, instrumental apparatus, and our model to fit the data. Then, we present and discuss the time- and frequency-resolved SFS data in both spectral regions for DS^- adsorbed on the interface of nanoscopic oil droplets.

EXPERIMENTAL AND THEORETICAL METHODS

Sample Preparation. Dispersions of oil droplets were prepared with 1 v/v % of deuterated hexadecane (hexadecane-d_{34}, 98% d, Cambridge Isotope) in aqueous solutions of 8 mM of sodium dodecyl sulfate (SDS, 99%, Biomol) in D_2O (99%, Sigma-Aldrich) as described in detail in ref 19. The solutions were mixed with a hand-held homogenizer (TH, OMNI International) and subsequently ultrasonicated (Sonorex DK

Received: December 2, 2013
Revised: February 27, 2014
Published: March 3, 2014

   dx.doi.org/10.1021/jp411798s | J. Phys. Chem. B 2014, 118, 3366−3371

156 BP). The size distribution of the droplets was measured with dynamic light scattering (Zetasizer Nano ZS, Malvern). The droplets had a mean diameter of ∼250 nm with a polydispersity index (PDI) of ∼0.2.

Sum-Frequency-Scattering Setup. Our experimental setup, which can be used to measure both time- and frequency-resolved SFS signals, is based on a femtosecond Ti:Sa amplifier system (Spitfire Pro 7W, Spectra Physics) producing pulses at a wavelength of 800 nm, with a pulse duration of 90 fs (full with at half maximum, fwhm), a pulse energy of 7 mJ, and a repetition rate of 1 kHz. The majority of the pulse energy is used to drive an optical parametric amplifier (OPA, HE-Topas-C, Light Conversion) that ultimately produces tunable infrared (IR) pulses (2.5−15 μm, 1−120 μJ) by difference frequency generation. The second visible (VIS) beam for the SF generation is derived from the fundamental amplifier output. A combination of a grating and a mechanical slit were used to control the pulse length and the bandwidth of the VIS pulses.

SFS signals were measured using the broadband IR laser pulses centered at ∼2900 or ∼1050 cm^{-1} (120 cm^{-1} fwhm bandwidth) and VIS pulses at 800 nm (fwhm bandwidth of 12 cm^{-1} for frequency-resolved and 185 cm^{-1} for time-resolved measurements). IR and VIS pulses were focused with a parabolic gold mirror (f = 100 mm) and a plano-convex lens (f = 125 mm), respectively. The beams were overlapped under an angle of β = 20° (measured in air) in a quartz sample cuvette (Hellma 106-QS with a path length of 100 or 200 μm) containing the sample dispersion. The entrance window was replaced by a CaF_2 window with a thickness of 1.3 mm, for the sample to be accessible to the IR light with a frequency > 1000 cm^{-1}. At a scattering angle of θ = 60° with respect to the direction of momentum conservation (measured in air), the scattered SF light was collimated with a plano-convex lens (f = 15 mm, Thorlabs LA1540-B) and then passed through two short wave pass filters (third Millenium, 3RD770SP). The SF light was spectrally dispersed with a monochromator (Acton, SpectraPro 2300i) and detected with an intensified CCD camera (ICCD, Princeton Instruments, PI-Max3) using a gate width of 10 ns. A Glan-Taylor prism (Thorlabs, GT15-B), a half-wave plate (EKSMA, 460-4215) in combination with a polarizing beam splitter cube (CVI, PBS-800-0050), and two BaF_2 wire grid polarizers (Thorlabs, WP25H-B) were used to control the polarization of the SF, VIS, and IR beams, respectively. Polarization combinations are labeled by three letter combinations of s and p (⊥ and ∥ to scattering plane) in the order of SF, VIS, and IR beams. For instance, ssp refers to the SF and VIS beams being polarized perpendicular to the scattering plane and the IR beam being polarized parallel to the scattering plane.

Frequency-resolved measurements were performed by overlapping the broadband IR pulses with narrowband VIS pulses (fwhm 12 cm^{-1}). Time-resolved data was measured using broadband IR and broadband VIS (fwhm 185 cm^{-1}) pulses. The IR−VIS delay time was controlled with a retro-reflector mirror mounted on a stepper-motor-driven translation stage (Thorlabs, LTS300). To probe the dephasing of the molecular vibrations, we employed the time-domain free induction decay (TD-FID) scheme previously described in refs 11−13. A femtosecond IR pulse first creates a vibrational coherence, i.e., a first-order polarization in the sample, which in turn is upconverted by a delayed short visible pulse. The upconversion results in the emission of SF photons that are scattered into the detector (Figure 1a,b). For FID traces, the intensity on the ICCD was integrated over all frequencies and the delay time

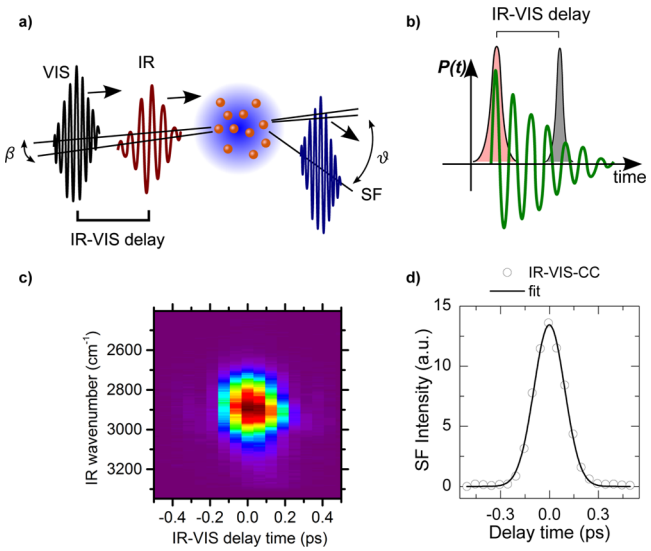

Figure 1. (a) Scheme showing the arrangement of femtosecond pulses in the time-resolved sum-frequency-scattering experiment. (b) Scheme showing the temporal order of the IR (red) and VIS (gray) pulses and the induced polarization (green). (c) Frequency-resolved cross-correlation (XFROG) of IR and VIS pulses and (d) spectrally integrated IR−VIS cross-correlation from a gold substrate in reflection (ppp polarization combination).

was scanned using time steps of 30−100 fs. For each measurement, several scans were averaged to reduce noise. To determine the time resolution of our system, we measured the frequency-resolved IR−VIS SF cross-correlation (XFROG), which is analogous to a FROG measurement,[23] from a gold substrate in reflection geometry. The incident angles of IR and VIS beams with respect to the surface normal were 40° and 60°, respectively. The generated SF beam was collimated and then detected in the same way as the scattered light in the scattering geometry. Figure 1c shows the SF spectrum as a function of the IR−VIS delay time (XFROG-trace). The shape of the XFROG trace is almost spherical, which confirms that IR and VIS pulses are not chirped. A conventional cross-correlation was obtained by integrating the XFROG trace along the frequency axis. The retrieved IR−VIS cross-correlation (fwhm of 220 fs) represents the instrument response function that can be well described with a Gaussian function (Figure 1d). The measured instrument response underestimates the actual time resolution of the measurement: The geometry used for the XFROG trace introduces a lengthening of the cross-correlation due to the noncollinear geometry. The geometric lengthening can be described by a Gaussian transfer function with a fwhm of 100 fs. This estimate is based on the beam geometry described above and the overlapping area of VIS and IR beams. In the scattering geometry, we use a sample cuvette that is placed such that its entrance and exit windows are tilted by 45° with respect to the IR beam. Because of refraction at the air/CaF_2/water interfaces, the effective overlapping angle β is reduced to ∼6° inside the sample cell. This reduction improves the time resolution of the experiment, yielding an actual time resolution of ∼200 fs. For the experiments in the spectral fingerprint region around 1000 cm^{-1}, the IR pulse becomes chirped because of the larger

dx.doi.org/10.1021/jp411798s | J. Phys. Chem. B 2014, 118, 3366−3371

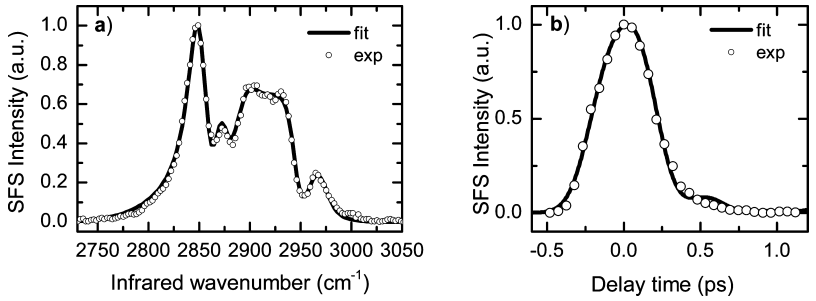

Figure 2. (a) Frequency-domain and (b) time-domain (FID) SFS signal of the methyl and methylene vibrational modes of DS^- ions at the aqueous interface of nanoscopic hexadecane-d_{34} droplets. Circles represent experimental data points and solid lines are simultaneous fits to both data sets using the model described in the methods section.

dispersion of D_2O[24] in this frequency range. This would lead to a reduced time resolution in the spectral fingerprint region. However, we can utilize the input CaF_2 window to partly cancel the lengthening of the IR pulse: Whereas the D_2O group velocity dispersion is normal, i.e., $n''(\omega) > 0$, the CaF_2 window is anomalously dispersive, i.e., $n''(\omega) < 0$. The true instrument response in the spectral fingerprint region can here be obtained from the rise time of the FID signal in the scattering experiments. We estimate the time resolution to be ~270 fs for the measurements in this spectral region.

Modeling of the Time- and Frequency-Domain Response. The interfacial response can be described with time domain (TD) and frequency domain (FD) response functions.[25] For the employed scheme (Figure 1b) and the samples studied here, the molecular response is only resonant to the IR light. The surface response function $\chi^{(2)}$ in the FD is generally modeled as a superposition of Lorentzians and a nonresonant response.[26] To obtain the response of the droplet surface, the local polarization needs to be multiplied by a phase factor and integrated over the droplet surface. This results in an effective particle susceptibility $\Gamma^{(2)}$, which consists of a sum of second-order susceptibility elements that are weighted by droplet shape and size dependent form factor functions.[27,28] Because surface and droplet response functions are related by linear transformations,[29] the effective susceptibility preserves the form of a sum of Lorentzians and a nonresonant part:

$$\Gamma^{(2)}(\omega) \propto A_{NR} e^{i\phi_{NR}} + \sum_j \frac{A_j}{\omega - \omega_j + i\gamma_j}$$

Here, A_{NR} and ϕ_{NR} are the amplitude and (relative) phase of the nonresonant contribution. A_j, ω_j, and γ_j are the amplitudes, frequencies, and the damping constants of the molecular vibration j. It is noteworthy that the transformation from the surface to the droplet response mixes different $\chi^{(2)}$-components; this generally leads to different observed phase relations and amplitude ratios of the vibrational modes compared to those obtained from planar SFG measurements.

An effective TD response function $R^{(2)}(t)$ is given by the Fourier transform of the effective susceptibility in the FD. The integration over the droplet surface is in this way implicitly included in the amplitudes A_j and A_{NR}. As in the case of planar SFG,[12,17,18] the TD response function $R^{(2)}(t)$ comprises a sum of exponentially decaying oscillators and an instantaneous nonresonant part:

$$R^{(2)}(t) \propto A_{NR} e^{i\phi_{NR}} \delta(t) - i\Theta(t) \sum_j A_j \exp(-i\omega_j t - \gamma_j t) + cc$$

Here, $\delta(t)$ is the Dirac delta function, and $\Theta(t)$ is the Heaviside step function. For the SFS measurements in the CH spectral region, the nonresonant response has been found to be slightly frequency-dependent.[30] For this spectral region, we therefore modeled the "nonresonant" response as a (truncated) Gaussian centered at 2533 cm^{-1} with fwhm of 530 cm^{-1}, as obtained from a fit to the measurements presented in ref 30. Although the complex response functions in the time and frequency domain are each others Fourier transform, the SFS signal obtained from the time- and frequency-resolved measurements possesses complementary information; the difference in the experimental schemes, e.g., the different pulse shapes of the VIS pulse, render the two measurement types sensitive to different aspects of the molecular interfacial response. This advantage of the combined measurement in the TD and FD SFS will be discussed in the next section.

The induced effective polarization of the droplet for a certain IR–VIS delay time τ is given by

$$P^{(2)}(t,\tau) \propto E_{VIS}(t - \tau) \int_{-\infty}^{\infty} E_{IR}(t-t') R^{(2)}(t') \, dt'$$

The time-resolved SFS signal is then proportional to the time integral of the squared induced effective polarization

$$I_{SFS\text{-}TD}(\tau) \propto \int_{-\infty}^{\infty} |P^{(2)}(t,\tau)|^2 \, dt$$

For the frequency-resolved experiment, the measured intensity at the sum frequency ω_{SF} is given by[17]

$$I_{SFS\text{-}FD}(\omega_{SF}) \propto \left| \int_{-\infty}^{\infty} E_{VIS}(\omega_{SF} - \omega_{IR}) \, E_{IR}(\omega_{IR}) \, \Gamma^{(2)}(\omega_{IR}) \, d\omega_{IR} \right|^2$$

To describe the data, we assumed Gaussian pulse shapes for the electric field of the VIS and the IR pulses,

$$E(t) = \frac{1}{2}\mathcal{E}(t)e^{-i\omega_0 t} + cc = \frac{1}{2\pi}\int_{-\infty}^{\infty} E(\omega)e^{-i\omega t} \, d\omega$$

with $\mathcal{E}$ being a complex amplitude that models the temporal shape of the Gaussian pulse with pulse length $\tau = \tau_{fwhm}/2(\log 2)^{1/2}$, and a possible chirp which is described by the chirp parameter a,[31]

$$\mathcal{E}(t) = \mathcal{E}_0 e^{-(1+ia)(t/\tau)^2}$$

The pulse lengths of VIS and IR pulses were estimated from the autocorrelation of the VIS pulse and the IR–VIS cross-correlation measured with a nonresonant gold substrate. The retrieved values were used as input parameters to fit the

dx.doi.org/10.1021/jp411798s | J. Phys. Chem. B 2014, 118, 3366–3371

spectrum and the FID simultaneously by adjusting the amplitudes, center frequencies and damping constants of the resonances mentioned below. We additionally introduced the linear chirp described by a as a fitting parameter to account for a possible chirp of the IR electric field due to the dispersion of D_2O and CaF_2. To estimate confidence intervals for the parameters, we used a bootstrapping method.[32]

RESULTS AND DISCUSSION

C−H Stretch Spectral Region. We measured TD and FD SFS from a dispersion of nanoscopic amphiphile-stabilized hexadecane-d_{34} droplets in D_2O. The bulk concentration of the amphiphile dodecyl sulfate (DS^-) was 8 mM. We measured the SFS spectrum (Figure 2a) and the free induction decay (Figure 2b) of the DS^- ions adsorbed at the interface of the droplets. Figure 2 shows the methyl and methylene vibrational SFS response of DS^-. The signal originates from the DS^- ions alone, because the deuterated methyl and methylene groups of the oil phase vibrate at lower frequencies.[33] Figure 2a depicts the SFS intensity spectrum in ppp polarization combination (i.e., all beams are polarized parallel to the scattering plane). The spectrum was fitted using the symmetric methylene (d^+, ~2850 cm^{-1}) and methyl (r^+, ~2869 cm^{-1}) stretch modes, the antisymmetric methylene (d^-, ~2925 cm^{-1}) and methyl (r^-, ~2965 cm^{-1}) stretch modes and the Fermi resonances of the above symmetric stretch modes with bending overtones (d^+_{FR}, ~2890 cm^{-1}; r^+_{FR}, ~2941 cm^{-1}). The center frequencies are consistent with previously reported center frequencies, as for instance in refs 18, 34, and 35. Figure 2b displays the time-resolved SFS signal of the same sample dispersion as in Figure 2a. Here, the ppp intensity has been integrated and recorded as a function of the IR−VIS delay time. The curve represents a first demonstration of a time-domain SF scattering measurement; it shows the free induction decay (dephasing) of the C−H vibrational modes of interfacial DS^- ions. We observed a fast dephasing with characteristic decay time of ~0.5 ps, which can be explained by the great number of modes that are simultaneously excited by the broadband IR pulse. Although the vibrational dephasing time of a single C−H stretch mode is of the order of 1 ps,[12,17,18,36] the interference of the modes results in a faster overall decay of the total polarization.

Using the model described above, we were able to simultaneously fit both time and frequency-resolved data assuming the above-mentioned resonances and an additional weakly frequency-dependent nonresonant response, as discussed in the modeling section. The fitting parameters are given in Table 1. The d^- mode was found to be out of phase with the other modes. This demonstrates the advantage of the combined measurement in time and frequency domains.[37] Although the frequency domain measurement could be fitted well with all resonances being in phase, this resulted in a poor fit to the time domain data. The time-resolved response is thus indeed more sensitive to the relative phases of the resonances,[12] adding valuable information to the spectral measurement. Residual differences between the model and the measured data might be attributed to higher order dispersive contributions or to IR absorption on the red side of the spectrum.[24] A small variation of the amplitude ratio (~10%) of d^+ to r^+ already suppresses the slight increase in the SFS signal at a delay time of ~0.55 ps. Moreover, some phenomena such as frequency-dependent local field factors might result in phase differences other than 0 or π of the vibrational oscillators.[26] Although such effects should be small compared to SFG measurements on metal substrates, they might give rise to the observed differences between model and data. In such cases, complex Fourier filtering methods may help to restrict the ranges of fit parameters.[38] Furthermore, it should be noted that amplitude ratios and the sign of the amplitudes of the vibrations are generally different in SFS measurements as compared to planar SFG measurements because different surface susceptibility components mix when transforming to the effective scattering susceptibility.[27,29]

Table 1. Parameters Obtained from the Fitting to the Time- and Frequency-Resolved Data in the CH-Stretch Spectral Region[a]

mode	ω (cm^{-1})	γ (cm^{-1})	A/A_{d+}
d^+	2850 ± 2	7 ± 1	1
r^+	2869 ± 4	4 ± 1	0.31 ± 0.1
d^-	2925 ± 5	16 ± 2	−2.4 ± 0.2
r^-	2965 ± 11	10 ± 9	1.6 ± 0.3
d^+_{FR}	2890 ± 3	17 ± 4	2.1 ± 0.2
r^+_{FR}	2941 ± 3	4 ± 1	0.6 ± 0.2
A_{NR}/A_{d+}	8.7 ± 2.0		
ϕ_{NR} (deg)	236 ± 11		

[a]Amplitudes are given relative to the amplitude of the d^+ mode. Confidence intervals are given as ± one standard deviation.

Vibrational Fingerprint Region. In addition to the measurements in the C−H stretch region, the droplet interfaces in the dispersion can be probed in the spectral fingerprint region around 1000 cm^{-1}, in which the symmetric stretch mode of the sulfate headgroup ($-SO_3^-$) is sum-frequency-active.[39] Figure 3a shows the SFS spectrum of the spectral fingerprint region, which was normalized by the spectrum of the broadband IR pulse. It displays a strong resonance at 1065 cm^{-1}, which we assign to the symmetric stretch mode of the headgroup. Additionally, a weak shoulder at lower frequencies (~960−1040 cm^{-1}) is visible. To further investigate this feature, we tuned the IR pulse further to the red side of the spectrum. The resulting spectrum and the corresponding FID are shown in Figure 3b,c. The spectral signature exhibits both the resonance of the sulfate headgroup and a second vibrational mode at 998 cm^{-1}. This second mode is even more apparent in the time-resolved measurement; its interference with the sulfate stretch mode results in a coherent beating of the FID signal with a beating period of ~450 fs. The corresponding difference frequency of 67 cm^{-1} fits well with the measured spectrum. The additional mode we observed has not been reported yet in SFG studies; nonetheless, the detected beating signal corroborates the evidence already seen in the frequency-resolved data. We suggest that the broader signal at 998 cm^{-1} originates from the C−O−S stretch band. Evidence for such a band in this frequency range has previously been reported in IR and Raman studies.[40,41]

As for the CH-stretch spectral region, we fitted TD and FD data simultaneously. The results are summarized in Table 2. Due to the dispersion of both the CaF_2 window and D_2O, we used a fit parameter for the linear chirp a to include the possibility of some linear chirp of the exciting IR pulse. However, as already pointed out in the methods section, the influences of the two dispersive media most likely cancel: The fit was not very sensitive to the chirp of the IR electric field and hence the data was fitted with a set to zero. The residual deviations to the measured data might arise from higher order dispersive contributions. Those contributions are more

dx.doi.org/10.1021/jp411798s | J. Phys. Chem. B 2014, 118, 3366−3371

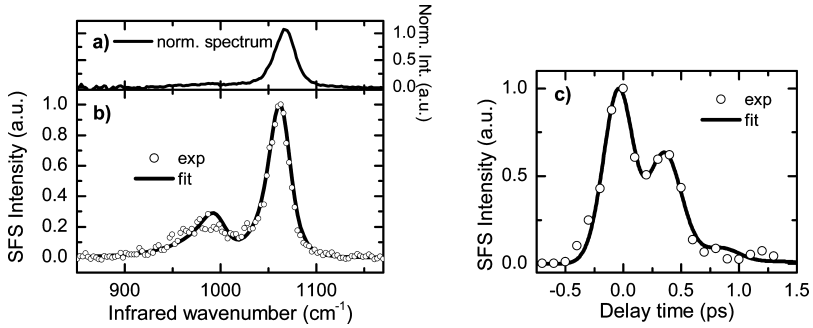

Figure 3. (a) IR-normalized spectrum of adsorbed DS^- ions in the spectral fingerprint region (ssp polarization combination, IR center frequency ~1050 cm^{-1}). It shows the symmetric stretch vibration of the sulfate headgroup and weak shoulder at lower frequencies. (b) and (c) show the frequency-domain (b) and time-domain (FID) (c) SFS signal when tuning the exciting IR pulse central frequency to ~1000 cm^{-1} . This enhances the influence of the mode at 998 cm^{-1}. Circles represent experimental data points, and solid lines are simultaneous fits to the data using the model described in the methods section.

Table 2. Parameters Obtained from the Fitting to the Time- and Frequency-Resolved Data in the SO-Stretch (Spectral Fingerprint) Region[a]

mode	ω(cm^{-1})	γ (cm^{-1})	$A/A_{SO_3\ ss}$
SO_3 ss	1065 ± 3	8.7 ± 1.3	1
COS	998.0 ± 5	14.3 ± 11.4	0.38 ± 0.12
$A_{NR}/A_{SO_3\ ss}$	0.09 ± 0.03		
ϕ_{NR} (deg)	214 ± 30		

[a]Confidence intervals are given as ± one standard deviation.

pronounced in the low frequency side of the spectrum, where the deviation of the model to the data is slightly larger.

CONCLUSIONS

In summary, we demonstrate a time-domain sum-frequency-scattering experiment. We measured the free induction decay of vibrational modes of amphiphilic molecules that were adsorbed onto the interface of nanoscopic hexadecane droplets in aqueous solution. Both the alkyl C−H stretch response and the response in the spectral fingerprint region were measured. Coherent beating effects between vibrational modes could be observed, strongly suggesting a sum-frequency-active C−O−S vibrational mode around 998 cm^{-1}. This time-domain SF study in a scattering geometry opens up possibilities to study dynamics of molecules at liquid−liquid interfaces, nanoscopic particle interfaces, and biological interfaces in aqueous solutions.

AUTHOR INFORMATION

Corresponding Author

*S. Roke: e-mail, sylvie.roke@epfl.ch.

Notes

The authors declare no competing financial interest.

ACKNOWLEDGMENTS

This work is supported by the Julia Jacobi Foundation, the Swiss National Science Foundation (grant number 200021_140472), and the European Research Council (grant number 240556).

REFERENCES

(1) Zanni, M. T.; Hochstrasser, R. M. Two-Dimensional Infrared Spectroscopy: A Promising New Method for the Time Resolution of Structures. *Curr. Opin. Struct. Biol.* **2001**, *11*, 516−522.
(2) Eisenthal, K. B. Liquid Interfaces Probed by Second-Harmonic and Sum-Frequency Spectroscopy. *Chem. Rev.* **1996**, *96*, 1343−1360.
(3) Arnolds, H. Vibrational dynamics of adsorbates Quo vadis? *Prog. Surf. Sci.* **2011**, *86*, 1−40.
(4) Matsumoto, Y.; Watanabe, K. Coherent Vibrations of Adsorbates Induced by Femtosecond Laser Excitation. *Chem. Rev.* **2006**, *106*, 4234−4260.
(5) Han, X.; Balgar, T.; Hasselbrink, E. Vibrational Dynamics of Hydrogen on Ge Surfaces. *J. Chem. Phys.* **2009**, *130*, 134701.
(6) Yamaguchi, S.; Tahara, T. Interface-Specific $\chi^{(4)}$ Coherent Raman Spectroscopy in the Frequency Domain. *J. Phys. Chem. B* **2005**, *109*, 24211−24214.
(7) Chen, J.; Kubota, J.; Wada, A.; Kondo, J. N.; Domen, K. Time-Resolved Sum Frequency Generation Reveals Adsorbate Migration between Different Surface Active Sites on Titanium Oxide/Pt(111). *J. Am. Chem. Soc.* **2009**, *131*, 4580−4581.
(8) Hsieh, C.; Campen, R. K.; Vila Verde, A. C.; Bolhuis, P.; Nienhuys, H.; Bonn, M. Ultrafast Reorientation of Dangling OH Groups at the Air-Water Interface Using Femtosecond Vibrational Spectroscopy. *Phys. Rev. Lett.* **2011**, *107*, 116102.
(9) Vidal, F.; Tadjeddine, A. Sum-Frequency Generation Spectroscopy of Interfaces. *Rep. Prog. Phys.* **2005**, *68*, 1095−1127.
(10) Arnolds, H.; Bonn, M. Ultrafast Surface Vibrational Dynamics. *Surf. Sci. Rep.* **2010**, *65*, 45−66.
(11) Guyot-Sionnest, P. Coherent Processes at Surfaces: Free-Induction Decay and Photon Echo of the Si-H Stretching Vibration for H/Si(111). *Phys. Rev. Lett.* **1991**, *66*, 1489−1492.
(12) Roke, S.; Kleyn, A. W.; Bonn, M. Time- vs. Frequency-Domain Femtosecond Surface Sum Frequency Generation. *Chem. Phys. Lett.* **2003**, *370*, 227−232.
(13) Owrutsky, J. C.; Culver, J. P.; Li, M.; Kim, Y. R.; Sarisky, M. J.; Yeganeh, M. S.; Yodh, A. G.; Hochstrasser, R. M. Femtosecond Coherent Transient Infrared Spectroscopy of CO on Cu(111). *J. Chem. Phys.* **1992**, *97*, 4421−4427.
(14) Roke, S.; Kleyn, A. W.; Bonn, M. Ultrafast Surface Dynamics Studied with Femtosecond Sum Frequency Generation. *J. Phys. Chem. A* **2001**, *105*, 1683−1686.
(15) Bonn, M.; Hess, C.; Wolf, M. The Dynamics of Vibrational Excitations on Surfaces: CO on Ru(001). *J. Chem. Phys.* **2001**, *115*, 7725−7735.
(16) Bordenyuk, A. N.; Benderskii, A. V. Spectrally- and Time-resolved Vibrational Surface Spectroscopy: Ultrafast Hydrogen-bonding Dynamics at D2O/CaF2 Interface. *J. Chem. Phys.* **2005**, *122*, 134713.

(17) Bordenyuk, A. N.; Jayathilake, H.; Benderskii, A. V. Coherent Vibrational Quantum Beats as a Probe of Langmuir-Blodgett Monolayers. *J. Phys. Chem. B* **2005**, *109*, 15941−15949.
(18) Nihonyanagi, S.; Eftekhari-Bafrooei, A.; Borguet, E. Ultrafast Vibrational Dynamics and Spectroscopy of a Siloxane Self-assembled Monolayer. *J. Chem. Phys.* **2011**, *134*, 084701.
(19) de Aguiar, H. B.; de Beer, A. G. F.; Strader, M. L.; Roke, S. The Interfacial Tension of Nanoscopic Oil Droplets in Water Is Hardly Affected by SDS Surfactant. *J. Am. Chem. Soc.* **2010**, *132*, 2122−2123.
(20) Strader, M. L.; de Aguiar, H. B.; de Beer, A. G. F.; Roke, S. Label-Free Spectroscopic Detection of Vesicles In Water Using Vibrational Sum Frequency Scattering. *Soft Matter* **2011**, *7*, 4959−4963.
(21) Jena, K. C.; Scheu, R.; Roke, S. Surface Impurities Are Not Responsible For the Charge on the Oil/Water Interface: A Comment. *Angew. Chem., Int. Ed. Engl.* **2012**, *51*, 12938−12940.
(22) de Aguiar, H. B.; Scheu, R.; Jena, K. C.; de Beer, A. G. F.; Roke, S. Comparison of Scattering and Reflection SFG: A Question of Phase-Matching. *Phys. Chem. Chem. Phys.* **2012**, *14*, 6826−6832.
(23) Trebino, R. *Frequency-Resolved Optical Gating: The Measurement of Ultrashort Laser Pulses*; Springer: New York, 2000; pp 101−115.
(24) Bertie, J. E.; Ahmed, M. K.; Eysel, H. H. Infrared Intensities of Liquids. 5. Optical and Dielectric Constants, Integrated Intensities, and Dipole Moment Derivatives of Water and Water-D2 at 22 deg C. *J. Phys. Chem.* **1989**, *93*, 2210−2218.
(25) Mukamel, S. *Principles of Nonlinear Optical Spectroscopy*; Oxford University Press: New York, 1995.
(26) Busson, B.; Tadjeddine, A. Non-Uniqueness of Parameters Extracted from Resonant Second-Order Nonlinear Optical Spectroscopies. *J. Phys. Chem. C* **2009**, *113*, 21895−21902.
(27) Roke, S.; Bonn, M.; Petukhov, A. V. Nonlinear Optical Scattering: The Concept of Effective Susceptibility. *Phys. Rev. B* **2004**, *70*, 115106.
(28) de Beer, A. G. F.; Roke, S. Sum frequency generation scattering from the interface of an isotropic particle: Geometrical and chiral effects. *Phys. Rev. B* **2007**, *75*, 245438.
(29) de Beer, A. G. F.; Roke, S. Obtaining molecular orientation from second harmonic and sum frequency scattering experiments in water: Angular distribution and polarization dependence. *J. Chem. Phys.* **2010**, *132*, 234702.
(30) de Aguiar, H. B.; Strader, M. L.; de Beer, A. G. F.; Roke, S. Surface Structure of Sodium Dodecyl Sulfate Surfactant and Oil at the Oil-in-Water Droplet Liquid/Liquid Interface: A Manifestation of a Nonequilibrium Surface State. *J. Phys. Chem. B* **2011**, *115*, 2970−2978.
(31) Diels, J.; Rudolph, W. *Ultrashort Laser Pulse Phenomena*; Optics and photonics; Elsevier Science: Amsterdam, 2006.
(32) Efron, B.; Tibshirani, R. *An Introduction to the Bootstrap*; Chapman & Hall/CRC Monographs on Statistics & Applied Probability; Taylor & Francis: London, 1994.
(33) Tyrode, E.; Hedberg, J. A Comparative Study of the CD and CH Stretching Spectral Regions of Typical Surfactants Systems Using VSFS: Orientation Analysis of the Terminal CH3 and CD3 Groups. *J. Phys. Chem. C* **2012**, *116*, 1080−1091.
(34) Lambert, A. G.; Davies, P. B.; Neivandt, D. J. Implementing the Theory of Sum Frequency Generation Vibrational Spectroscopy: A Tutorial Review. *Appl. Spectrosc. Rev.* **2005**, *40*, 103−145.
(35) Messmer, M. C.; Conboy, J. C.; Richmond, G. L. Observation of Molecular Ordering at the Liquid-Liquid Interface by Resonant Sum Frequency Generation. *J. Am. Chem. Soc.* **1995**, *117*, 8039−8040.
(36) Star, D.; Kikteva, T.; Leach, G. W. Surface Vibrational Coherence at the CaF2/Air Interface: Vibrational Wave Packet Dynamics as a Probe of Interface Inhomogeneity. *J. Chem. Phys.* **1999**, *111*, 14−17.
(37) Lagutchev, A.; Hambir, S. A.; Dlott, D. D. Nonresonant Background Suppression in Broadband Vibrational Sum-Frequency Generation Spectroscopy. *J. Phys. Chem. C* **2007**, *111*, 13645−13647.
(38) de Beer, A. G. F.; Chen, Y.; Scheu, R.; Conboy, J. C.; Roke, S. Analysis of Complex Spectra Using Fourier Filtering. *J. Phys. Chem. C* **2013**, *117*, 26582−26587.
(39) Johnson, C. M.; Tyrode, E. Study of the Adsorption of Sodium Dodecyl Sulfate (SDS) at the Air/Water Interface: Targeting the Sulfate Headgroup Using Vibrational Sum Frequency Spectroscopy. *Phys. Chem. Chem. Phys.* **2005**, *7*, 2635−2640.
(40) Picquart, M. Vibrational Model Behavior of SDS Aqueous Solutions Studied by Raman Scattering. *J. Phys. Chem.* **1986**, *90*, 243−250.
(41) Prosser, A. J.; Franses, E. I. Infrared Reflection Absorption Spectroscopy (IRRAS) of Aqueous Nonsurfactant Salts, Ionic Surfactants, and Mixed Ionic Surfactants. *Langmuir* **2002**, *18*, 9234−9242.